Proceedings of the
47th IEEE Conference on Decision and Control
Cancun, Mexico, Dec. 9-11, 2008

Dual actuation for high-bandwidth nanopositioning

Georg Schitter, Wouter F. Rijkée, and Nghi Phan

Abstract— **The imaging speed of atomic force microscopes (AFM) is limited by the bandwidth of the feedback loop to measure the sample topography. In contact mode as well as tapping mode operation, this feedback loop is crucial to control and minimize the force between the probing tip and the sample, which is done by controlling the vertical tip sample distance via a piezo actuator. For fast imaging, control of the probe-sample distance requires a high closed-loop bandwidth. To achieve this goal without reducing the existing positioning range, a second, high-bandwidth actuator is introduced to an existing AFM setup. A model-based controller is designed and implemented to improve the bandwidth of the primary feedback loop for tapping mode and contact mode imaging. For highest imaging bandwidth in contact mode, an accessory high-performance controller is designed and implemented on the dual actuated AFM system. The improved performance of the new control-system is experimentally demonstrated.**

I. INTRODUCTION

Ongoing research in material science and life sciences demand scanning probe based imaging systems that enable a high spatial and temporal resolution. The ultimate goal is to image biological systems on the molecular level at video rates of 25 images per second or even faster [1]. Recent break throughs demonstrated feasibility of video-rate imaging at line scan rates of up to 10 kHz at scan ranges from a few hundred nanometers [2], [3] up to several micrometers [4]. For faster scanning several improvements of the scanning motion by modern control methods have been successfully demonstrated [5]-[9], which for the current state of the art solved the problem of fast scanning.

Nowadays, the main limitation in most high-speed imaging applications is not the scanning motion, but the maximum bandwidth at which the feedback loop to measure the sample topography can track fast changing topographical features [1]. For some laboratory systems first attempts have been reported to improve the bandwidth of this measurement loop by hardware-modifications [2], [4], [10] or by utilizing modern control methods [11]. Improving the bandwidth of the vertical positioning system by replacing the standard actuator by a fast piezoelectric element has been reported [2], [4], but may not be beneficial for applications where a long stroke ($> 6\ \mu m$) of the Z-actuator is required. To overcome this limitation, first attempts have been reported to add a second Z-actuator [12]-[14], resulting in an dual actuated system. Here the main challenge is to control two competing feedback loops operating on the same system output [13], [14]. Dual actuation has been successfully demonstrated for a similar application in hard disk drives [15], [16]. Implementations to improve the bandwidth of the AFM feedback loop via modern control methods have been reported based on robust control [11], an internal model control approach [17], and a gain scheduling based approach [18]. These improvements have been implemented for single actuated AFM systems, ameliorating the bandwidth problem to a certain extent.

The main contribution of this paper is to demonstrate the benefit of model-based control for contact mode as well as tapping mode imaging, and to obtain an even higher bandwidth for contact mode imaging with a dual actuated AFM system using two piezo actuators with different frequency spectra. To this end the vertical positioning system of a commercial AFM is expanded by a second, fast actuator which allows for a high positioning bandwidth without reducing the vertical range of the commercial system. A model-based controller is implemented for the standard AFM as well as for the dual actuated system to demonstrate the benefit of the higher feedback bandwidth. Experimental results verify the improved performance of the resulting imaging system.

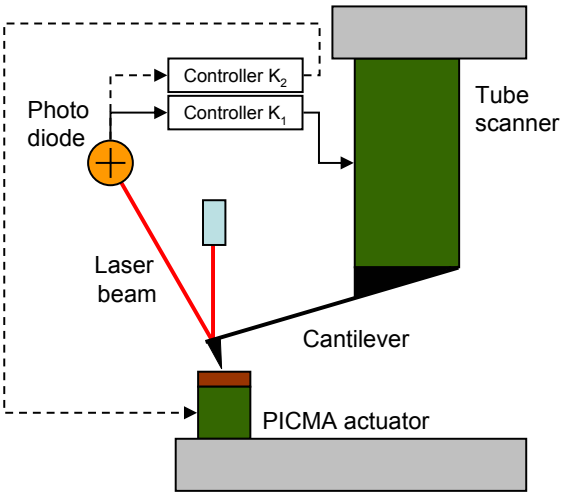

Fig. 1. Schematic of the AFM system. A tube scanner is used to perform the scanning motion and the vertical positioning of the standard AFM. The dashed lines indicate the second control loop for dual actuation.

II. SETUP AND MODELING

A commercially available AFM system (Dimension-AFM, Veeco, Santa Barbara, CA, USA) is used as basic setup for testing the new control system. This standard AFM

G. Schitter and W.F. Rijkée are with the Delft Center for Systems and Control, Delft University of Technology, 2628 CD Delft, The Netherlands.
N. Phan is with Veeco Metrology Inc., 112 Robin Hill Rd., Santa Barbara, CA-93117, USA
Corresponding author Email-address: g.schitter@tudelft.nl

is extended to a dual actuated system by introducing a second actuator for the vertical (Z-) direction, according to Figure 1. The auxiliary actuator is a PICMA stack-piezo (Physikinstrumente, Waldbronn, Germany) with a nominal first free resonance of >300 kHz.

For analysis of the system dynamics a model of the dual actuated system is required. The inputs to the system are the inputs of the power amplifiers for the individual actuators, according to Figure 2. The output of the system is the sum of the positions of the actuators, as both of them are affecting the tip-sample distance in the same way.

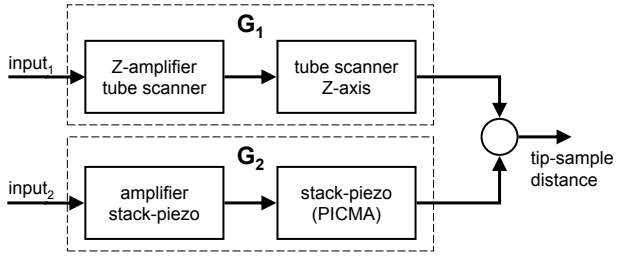

Fig. 2. Block diagram of the dual actuation for the vertical positioning axis of the AFM.

The subsystem G_1 represents the vertical positioning axis of the standard AFM, which is actuated by a tube scanner. The subsystem G_2 represents the auxiliary actuator and the corresponding custom made power amplifier for fast vertical positioning. The system output is given by the relative vertical position of the cantilever base and the sample surface. For characterizing the individual subsystems a cantilever has been brought in contact with a silicon sample, where the vertical deflection of the cantilever, measured by the AFM's photo-detector, corresponds to the system output. The free resonance frequency of the cantilever was >1 MHz, i.e. the cantilever dynamics do not influence the measured dynamics of the actuator.

A. Modeling of the tube scanner

A model for the standard AFM system (Dimension, Veeco, USA) in vertical direction is derived from a measured frequency response. A random noise signal is applied to the input of G_1 while recording the deflection signal of the cantilever by using a dynamic signal analyzer (HP35665A, Agilent, Palo Alto, CA, USA), which directly gives the frequency response of the characterized system. Figure 3 shows the measured Bode-plot of the tube scanner in Z-direction (black line), where the main resonance of the actuator occurs at 6.35 kHz.

A 10^{th} order model is fitted to the measured data, which is shown by the red line in Figure 3:

$$G_1 = \frac{K_T \cdot R_T \cdot \prod_{i=1}^{2}\left(s^2+2\zeta_{zi}\omega_{zi}s+\omega_{zi}^2\right)}{\prod_{j=1}^{3}\left(s^2+2\zeta_{pj}\omega_{pj}s+\omega_{pj}^2\right)} \qquad (1)$$

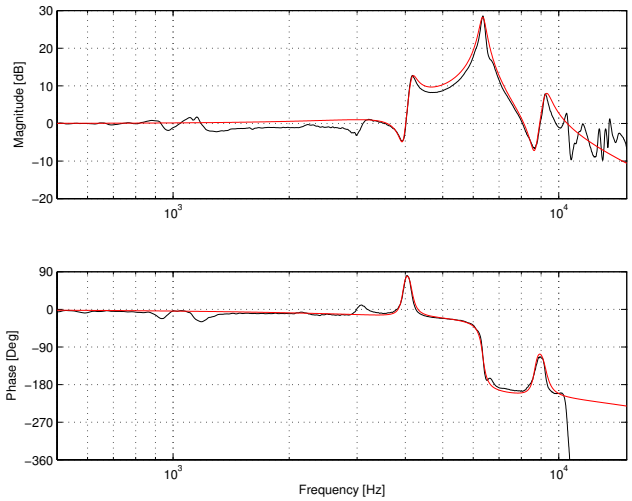

Fig. 3. Measured (black) and fitted (red) Bode-plot of the Z-actuator of the standard AFM system.

TABLE I

MODEL PARAMETERS FOR THE TUBE SCANNER MODEL G_1 IN EQ.(1).

index	ω_{index} [kHz]	ζ_{index}
z1	3.95	0.020
z2	8.67	0.022
p1	4.15	0.024
p2	6.35	0.020
p3	9.23	0.030

with gain $K_T = 2.0 \cdot 10^9$, a fourth order Padé approximation R_T of a 10 μs time delay, and undamped resonance and anti-resonances ω_{index} and the corresponding damping ratios ζ_{index} according to Table I.

B. Modeling of the fast actuator

The PICMA actuator, added to the vertical positioning system according to Fig. 2, has been characterized in the same way. Here the random noise signal has been applied to the input of G_2, while recording the deflection signal of the cantilever as the system output. Figure 4 shows the measured frequency response of the fast actuator (black line) along with a fitted 8^{th} order model (red line)

$$G_2 = \frac{K_P \cdot R_P \cdot \left(s^2+2\zeta_{z1}\omega_{z1}s+\omega_{z1}^2\right)}{\left(s^2+2\zeta_{p1}\omega_{p1}s+\omega_{p1}^2\right)\left(s^2+2\zeta_{p2}\omega_{p2}s+\omega_{p2}^2\right)} \qquad (2)$$

with gain $K_P = 1.6 \cdot 10^{12}$, a fourth order Padé approximation R_P of a 1.7 μs time delay, and undamped anti-resonance and resonances ω_l and the corresponding damping ratios ζ_l according to Table II.

III. CONTROLLER DESIGN

In this section, a new control system is developed that:

- enables a higher closed-loop bandwidth of the standard AFM system,
- allows faster imaging in contact and tapping mode, and

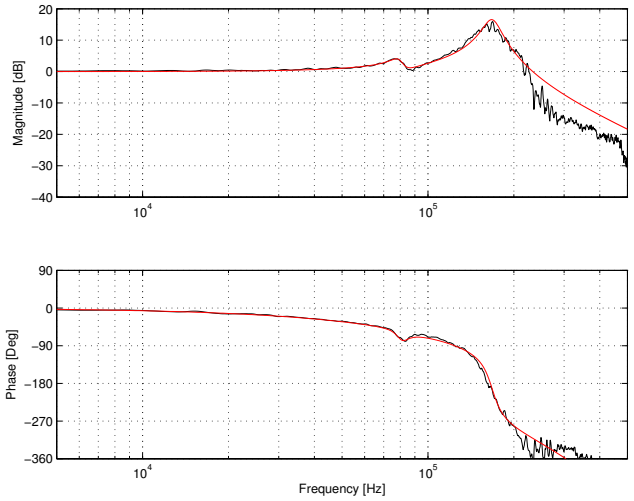

Fig. 4. Measured (black) and fitted (red) Bode-plot of the high-bandwidth actuator for the dual actuated positioner.

TABLE II

MODEL PARAMETERS FOR THE PICMA-ACTUATOR MODEL G_2 IN EQ.(2).

index l	ω_l [kHz]	ζ_l
z1	82	0.067
p1	80	0.060
p2	168	0.070

- achieves an even higher closed-loop bandwidth for contact mode imaging by dual actuation.

In order to address the first two points, a model-based controller is developed in the next section. The third point is addressed by extending the model-based controller for the standard AFM by an auxiliary feedback loop to control the second actuator.

The controller design is influenced by the available control hardware. The digital signal processor (DSP) of the standard AFM control system does not allow simple reprogramming and, therefore, a fixed model-based filter is added to the standard PI feedback loop, while keeping the tuning capability of the PI controller, in order to get good tracking performance for tapping mode as well as contact mode imaging. Since the real-time power of the DSP is not sufficient to also control the high-bandwidth feedback loop, the AFM system is extended by an external control hardware, in order to control the second actuator of the dual actuated AFM.

A. Model-based control of the tube scanner

The PI-controlled feedback loop of the standard AFM in vertical direction is limited in bandwidth by the resonance peak of the scanner (c.f. Fig. 3). To improve the PI-controlled feedback loop in both contact mode and tapping mode, this resonance-peak is reduced by adding a fixed model-based filter K_f in series with the PI-controller of the standard AFM (see Fig. 5). The PI-controller enables tuning the system during operation in order to achieve optimal surface tracking of the positioning system. In Fig. 5, the block G_1 represents the model of the tube scanner (Fig. 3). The block

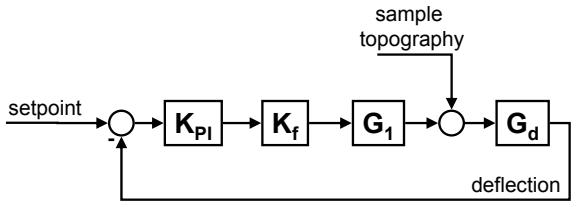

Fig. 5. Block diagram of the control-loop for the standard AFM system with the tube scanner as Z-actuator. K_{PI} represents the PI-controller and K_f is the model-based filter to extend the closed-loop bandwidth of the tube scanner in Z-direction. G_1 represents the Z-actuator and amplifier, and G_d is the deflection detection system.

G_d models the dynamics of the cantilever and deflection detection system, which can be modeled as a simple gain in contact mode [11] and as a first order low pass in tapping mode operation [19]. K_{PI} is the PI-feedback controller of the standard AFM, and K_f is a fourth order filter, containing two notches to suppress the scanner's resonances in Z-direction. Four poles are added to this filter in order to make K_f proper.

$$K_f = \frac{\left(s^2+2\zeta_{z1}\omega_{z1}+\omega_{z1}^2\right)\left(s^2+2\zeta_{z2}\omega_{z2}+\omega_{z2}^2\right)}{\left(s^2+2\zeta_{p1}\omega_{p1}+\omega_{p1}^2\right)\left(s^2+2\zeta_{p2}\omega_{p2}+\omega_{p2}^2\right)}, \quad (3)$$

with the parameters as listed in Table III.

TABLE III

PARAMETERS FOR THE LOOP SHAPING FILTER K_f.

index	ω_{index} [kHz]	ζ_{index}
z1	6.36	0.141
z2	6.69	0.127
p1	6.36	1
p2	6.69	0.316

The order of K_f has been limited to four, as this filter is implemented on the DSP of the AFM control system at a sampling rate of 100 kHz.

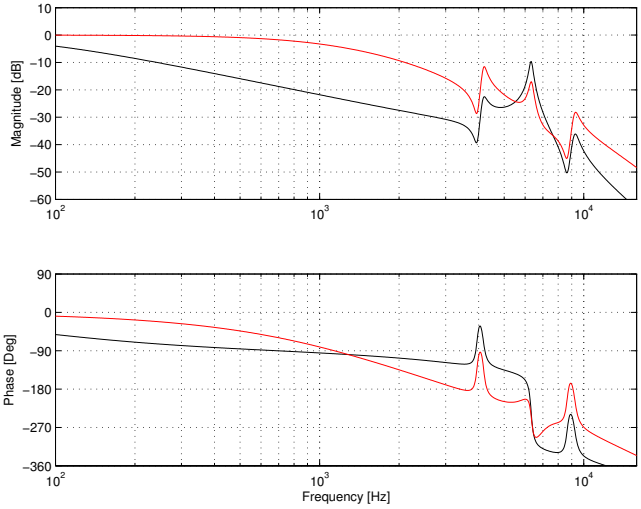

Fig. 6. Bode-diagram of the closed-loop PI-controlled (black) and the model-based controlled (red) AFM.

A comparison of the simulated closed-loop response of the PI-controlled and the model-based controlled AFM is shown in Figure 6. The -3dB bandwidth of the PI-controlled AFM without additional filters in the loop is below 100 Hz, while adding the filter K_f allows to improve the -3 dB bandwidth to 1 kHz while the gain margin is still higher than in the PI-controlled case. At the design of the model-based filter, attention has also been paid for a sufficient high phase margin in order to cope with the additional phase lag due to tapping mode operation.

B. Control of the PICMA actuator

The control system described in the previous section is extended by an auxiliary control-loop for the second actuator (see Fig. 2), in order to achieve an even higher closed-loop bandwidth. The scheme of the extended control system is shown in Figure 7.

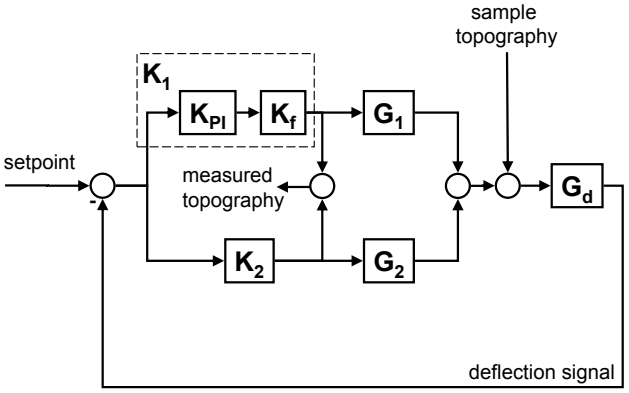

Fig. 7. Block diagram of the control-loop for the dual actuated positioning system. K_1 is the model-based controller for the standard AFM, K_2 is the controller for the auxiliary high-bandwidth actuator.

Based on the model given in Eq.(2) the feedback controller K_2 is designed in the H_∞-framework according to [11]. The closed-loop response of the feedback loop for the tube scanner (Fig. 8, red line) has been taken as basis when chosing the weighting functions for loop-shaping of the fast control-loop. For simplicity the gain of the deflection detection system G_d is set to 1.

The designed 11^{th} order controller is balanced and reduced to 5^{th} order

$$K_2 = \frac{2.1\cdot 10^5 \cdot \prod_{i=1}^{2}\left(s^2+2\zeta_{zi}\omega_{zi}+\omega_{zi}^2\right)}{(s+\omega_{p1})\cdot\prod_{j=2}^{3}\left(s^2+2\zeta_{pj}\omega_{pj}+\omega_{pj}^2\right)}, \qquad (4)$$

with the filter parameters listed in Table IV, resulting in the closed-loop response shown in Figure 8 (blue line).

Combining the controller from Section III-A with the controller for the PICMA actuator K_2 according to Figure 7 results in the closed-loop response of the dual actuated system as shown in Figure 8 (black line)

$$H_{cl} = \frac{G_d\left(G_1K_1+G_2K_2\right)}{1+G_d\left(G_1K_1+G_2K_2\right)}, \qquad (5)$$

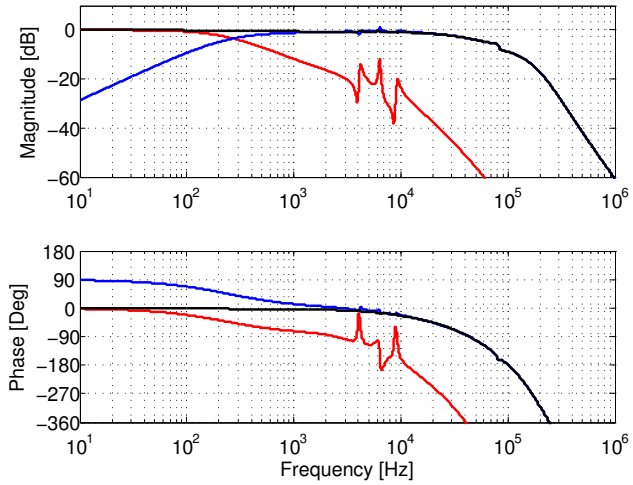

Fig. 8. Bode diagram of the closed-loop controlled dual actuated AFM system, showing the frequency response H_{cl} of the full system (black line), the feedback loop H_{cl1} of the tube scanner (red line), and the feedback loop H_{cl2} of the PICMA actuator (blue line).

TABLE IV
PARAMETERS FOR THE AUXILIARY FEEDBACK K_2.

index	ω_{index} [kHz]	ζ_{index}
z1	80.0	0.06
z2	168	0.07
p1	2.0	-
p2	81.2	0.07
p3	198	0.37

consisting of the loop for the piezo tube actuator (red line)

$$H_{cl1} = \frac{G_dG_1K_1}{1+G_d\left(G_1K_1+G_2K_2\right)}, \qquad (6)$$

and the loop for the PICMA actuator (blue line)

$$H_{cl2} = \frac{G_dG_2K_2}{1+G_d\left(G_1K_1+G_2K_2\right)}. \qquad (7)$$

Implementation of K_2: The bandwidth of the fast feedback loop is close to the 100 kHz sampling rate of the DSP and is beyond the DSP's available computing power. Therefore, K_2 is implemented on a field programmable analog array (FPAA), similar to the application described in [20]. The FPAA [21] allows the implementation of the 5^{th} order filter K_2 on a single chip. At the implementation, the controller K_2 has been re-tuned on the real AFM to achieve best control performance. The bandwidth of the FPAA allows for compensation of the resonance frequencies of the PICMA actuator occuring at 80 and 168 kHz.

IV. EXPERIMENTAL RESULTS

A. Tapping mode with model-based controlled tube scanner

Figure 9 shows a comparison between the PI-controlled AFM system and the model-based controlled AFM (tube scanner only) for imaging in tapping mode. The sample

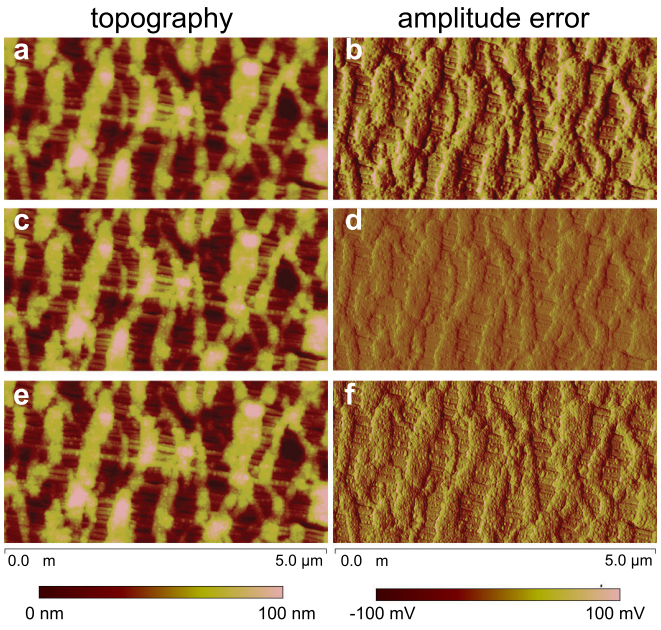

Fig. 9. Comparison between the PI-controlled AFM and the model-based control AFM, showing a Celgard membrane imaged in tapping mode. Topography (a) and amplitude error (b) recorded with the PI-controlled AFM at 4 lines per second; Topography (c and e) and amplitude error (d and f) recorded with the model-based controlled AFM at 4 and 11 Hz, respectively. All images are recorded at a resolution of 1024 pixels per line and 512 lines per image. Scaling is the same for all topography and error images, respectively, according to the scale bar at the bottom of the image.

under investigation is a Celgard membrane (Celgard, Charlotte, NC, USA). All images are recorded in tapping mode with a Si-cantilever (f_0 >1MHz, Q-factor $\approx$ 200) at a resolution of 1024 pixels per line and 512 lines per image. Images 9(a-b) are recorded with the PI-controlled AFM at a speed of 4 lines per second. Images 9(c-d) and 9(e-f) are recorded with the model-based controlled AFM at a speed of 4 and 11 lines per second, respectively. The higher closed loop bandwidth is obvious by the reduced amplitude error in case of the model-based controlled AFM system when imaging at the same speed of 4 lines per second. When imaging with the model based controlled AFM at 11 lines per second, i.e. more than 2.5 times faster, the residual control error is still lower than the one of the PI-controlled AFM at 4 lines per second.

B. Dual actuated system

Figure 10 shows a comparison between the PI-controlled AFM system (a and b), the model-based controlled standard AFM (c and d), and the dual actuated AFM (e and f) for imaging in contact mode. The sample shown is a Silicon calibration grating with 200 nm deep squared holes at a pitch of 10 μm, and is imaged at a speed of three lines per second with a Si-cantilever (f_0 >1 MHz) in contact mode. Operating the AFM with the PI-controller results in the largest cantilever deflection (Fig. 10.b), which denotes the residual control error. The deflection is significantly reduced

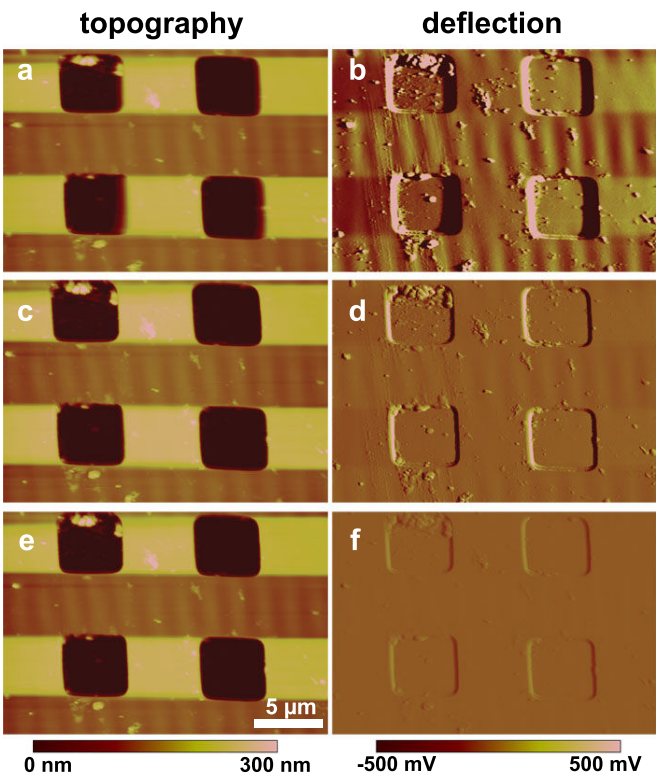

Fig. 10. Comparison of the residual control error between the standard AFM and the dual actuated system. All images were recorded at a line-scan rate of 3 Hz and a resolution of 512 by 512 pixel. Topography (a, c, and e) and deflection (b, d, and f) of the PI-controlled (a and b), model-based controlled tube scanner (c and d), and the dual actuated AFM system (e and f), respectively. Scaling is the same for all three topography and error images, respectively, according to the scale bar at the bottom of the image.

using the model-based controlled tube scanner (Fig. 10.d), and is even smaller in case of the dual actuated AFM system (Fig. 10.f).

Figure 11 shows cross sections of the error images given in Figure 10, allowing to quantify the reduction of the maximum cantilever deflection, corresponding to the maximum variation of the imaging force. The reduction of the cantilever deflection by dual actuation is clearly visible (Fig. 11, blue line). The maximum deflection signal at the photo-detector is reduced from 2200 mV of the PI-controlled AFM (black line) to about 100 mV in case of the dual actuated system (blue line). Please note also the loss of contact in case of the PI-controlled AFM where the negative deflection signal saturates at -1000 mV, which is the deflection of the free cantilever.

This considerable reduction of the cantilever deflection gives two main advantages: (i) the maximum error and the maximum variation of the imaging force is reduced, thus resulting in more reliable measurement data, and (ii) due to the significant reduction of the maximum negative cantilever deflection, the AFM can be operated closer to the minimum force point without loss of tip sample contact, thus reducing the average imaging force and preventing damage to the tip and sample.

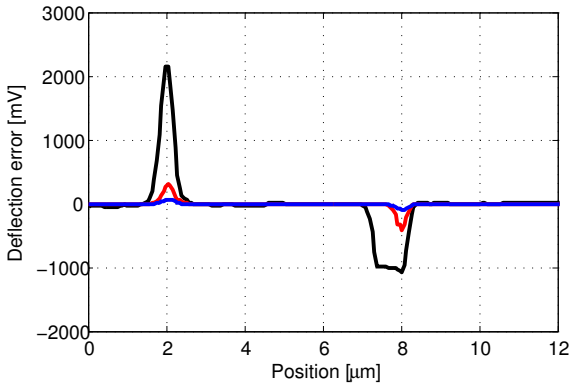

Fig. 11. Cross sections of the deflection images shown in Fig. 10(b, d, and f), showing the residual control error of the PI-controlled AFM (black line), the model-based controlled tube scanner (red line), and the dual actuated AFM (blue line) while imaging at a speed of 3 lines per second in contact mode.

V. CONCLUSIONS AND FUTURE WORKS

A. Conclusions

This paper presents a significant reduction of the residual tracking-error for topography measurement in atomic force microscopy. Model-based control of the tube scanner in the commercial AFM allows to improve the feedback bandwidth for both imaging modes, contact and tapping mode. Extending the vertical positioning system of the standard AFM with an auxiliary, high-bandwidth piezo actuator and controlling this dual actuated system with a model-based controller enables an even higher feedback bandwidth for contact mode imaging with reduced measurement error.

B. Future Works

Current research is focussed on the development of actuators and power amplifiers with extreme high bandwidths (>200 kHz) and the design and implementation of a multi-input-multi-output (MIMO) controller for the dual actuated AFM system. The development of an integrated control system that allows for a direct implementation of the designed MIMO controller at high sampling rates may allow to overcome the discussed hardware limitations. This may result in an even higher closed-loop bandwidth, which will further reduce the measurement error and enable higher imaging rates with the AFM.

VI. ACKNOWLEDGMENTS

The authors would like to thank Fritz Krainer and Jeff Markakis from Veeco for their support and fruitful discussions. This work has been supported by the Netherlands Organization for Scientific Research (NWO), Innovational Research Incentives Scheme (VENI DOV.7835), by the National Institutes of Health under Award RO1 GM065354, and by a research agreement with Veeco.

REFERENCES

[1] P. K. Hansma, G. Schitter, G. E. Fantner, and C. Prater, "High speed atomic force microscopy," *Science*, vol. 314, p. 601, 2006.

[2] T. Ando, T. Kodera, E. Takai, D. Maruyama, K. Saito, and A. Toda, "A high-speed atomic force microscope for studying biological macromolecules," *Proc. Nat. Acad. Sci.*, vol. 98, p. 12468, 2001.

[3] M. J. Rost, L. Crama, P. Schakel, E. V. Toll, G. B. E. M. V. Velzen-Williams, C. F. Overgauw, H. ter Horst, H. Dekker, B. Okhuijsen, M. Seynen, A. Vijfigischild, P. Han, A. J. Katan, K. Schoots, R. Schumm, W. van Loo, T. H. Oosterkamp, and J. W. M. Frenken, "Scanning probe microscopes go video rate and beyond," *Rev. Sci. Instr.*, vol. 76, p. 053710, 2005.

[4] G. Schitter, K. J. Åström, B. E. DeMartini, P. J. Thurner, K. L. Turner, and P. K. Hansma, "Design and modeling of a high-speed afm-scanner," *IEEE Trans. Contr. Syst. Technol.*, vol. 15, p. 906, 2007.

[5] D. Croft, G. Shed, and S. Devasia, "Creep, hysteresis, and vibration compensation for piezoactuators: Atomic force microscopy application," *ASME J. Dyn. Syst. Meas. Contr.*, vol. 128, p. 35, 2001.

[6] S. Salapaka, A. Sebastian, J. P. Cleveland, and M. V. Salapaka, "High bandwidth nano-positioner: A robust control approach," *Review of Scientific Instruments*, vol. 73, no. 9, p. 3232, 2002.

[7] Q. Zou, K. K. Leang, E. Sadoun, M. J. Reed, and S. Devasia, "Control issues in high-speed afm for biological applications: collagen imaging example," *Asian Journal of Control*, vol. 6(2), p. 164, 2004.

[8] A. Sebastian and S. M. Salapaka, "Design methodologies for robust nano-positioning," *IEEE Trans. Contr. Syst. Technol.*, vol. 13, p. 868, 2005.

[9] A. J. Fleming and S. O. R. Moheimani, "Sensorless vibration suppression and scan compensation for piezoelectric tube nanopositioners," *IEEE Trans. Contr. Syst. Technol.*, vol. 14, p. 33, 2006.

[10] J. H. Kindt, G. E. Fantner, J. A. Cutroni, and P. K. Hansma, "Rigid design of fast scanning probe microscopes using finite element analysis," *Ultramicroscopy*, vol. 100, p. 259, 2004.

[11] G. Schitter, A. Stemmer, and F. Allgöwer, "Robust two-degree-of-freedom control of an atomic force microscope," *Asian Journal of Control*, vol. 6, p. 156, 2004.

[12] D. Knebel, M. Amrein, K. Voigt, and R. Reichelt, "A fast and versatile scan unit for scanning probe microscopy," *Scanning*, vol. 19, p. 264, 1997.

[13] T. Sulchek, S. C. Minne, J. D. Adams, D. A. Fletcher, A. Atalar, C. F. Quate, and D. M. Adderton, "Dual integrated actuators for extended range high speed atomic force microscopy," *Appl. Phys. Lett.*, vol. 75, p. 1637, 1999.

[14] K. E. Rifai, O. M. E. Rifai, and K. Youcef-Toumi, "On dual actuation in atomic force microscopes," in *Proceedings of the 2004 American Control Conference*, AACC. Boston, MA: IEEE, June 30-July 2 2004, p. 3128.

[15] K. Mori, T. Munemoto, H. Otsuki, Y. Yamaguchi, and K. Akagi, "A dual-stage magnetic disk drive actuator using a piezoelectricdevice for a high track density," *IEEE Transactions on Magnetics*, vol. 27, no. 6, p. 5298, 1991.

[16] S. Koganezawa, Y. Uematsu, T. Yamada, H. Nakano, J. Inoue, and T. Suzuki, "Dual-stage actuator system for magnetic disk drives using a shearmode piezoelectric microactuator," *IEEE Transactions on Magnetics*, vol. 35, no. 2, p. 988, 1999.

[17] N. Kodera, H. Yamashita, and T. Ando, "Active damping of the scanner for high-speed atomic force microscopy," *Rev. Sci. Instrum.*, vol. 76, p. 053708, 2005.

[18] N. Kodera, M. Sakashita, and T. Ando, "Dynamic proportional-integral-differential controller for high-speed atomic force microscopy," *Rev. Sci. Instrum.*, vol. 77, p. 083704, 2006.

[19] J. Mertz, O. Marti, and J. Mlynek, "Regulation of a microcantilever response by force feedback," *Appl. Phys. Lett.*, vol. 62(19), p. 2344, 1993.

[20] G. Schitter and N. Phan, "Field programmable analog array (fpaa) based control of an atomic force microscope," in *Proceedings of the 2008 American Control Conference*, AACC. Seattle, WA: IEEE, June 11–13 2008, p. 2690.

[21] *Field Programmable Analog Array: AN231K04-DVLP3 - AnadigmApex Development Board*, Anadigm Inc., Campbell, CA, USA, 2006.